537

Study on mechanical performance of composite beam with innovative composite slabs

Yong Yang [1], Yunlong Yu [*1], Xianwei Zhou [1],
Charles W. Roeder [2] and Xudong Huo [1]

[1] *School of Civil Engineering, Xi'an University of Architecture & Technology, Xi'an, Shannxi 710055, China*
[2] *Civil and Environmental Department, University of Washington, Seattle, WA 98115, USA*

Abstract. A new type of composite beam which consists of a wide flange steel shape beam and an innovative type of composite slab was introduced. The composite slab is composed of concrete slab and normal flat steel plates, which are connected by perfobond shear connectors (PBL shear connectors). This paper describes experiments of two large-scale specimens of that composite beam. Both specimens were loaded at two symmetric points for 4-point loading status, and mechanical behaviors under hogging and sagging bending moments were investigated respectively. During the experiments, the crack patterns, failure modes, failure mechanism and ultimate bending capacity of composite beam specimens were investigated, and the strains of concrete and flat steel plate as well as steel shapes were measured and recorded. As shown from the experimental results, composite actions were fully developed between the steel shape and the composite slab, this new type of composite beams was found to have good mechanical performance both under hogging and sagging bending moment with high bending capacity, substantial flexure rigidity and good ductility. It was further shown that the plane-section assumption was verified. Moreover, a design procedure including calculation methods of bending capacity of this new type of composite beam was studied and proposed based on the experimental results, and the calculation methods based on the plane-section assumption and plastic theories were also verified by comparisons of the calculated results and experimental results, which were agreed with each other.

Keywords: flat steel plate-concrete composite slabs; composite beam; bending performance; bending capacity; experimental study

1. Introduction

Steel-concrete composite floor slabs have been utilized for their advantages in elements of construction such as avoiding formworks and temporary scaffoldings, and constructing several stories simultaneously. Composite slabs with profiled steel sheetings or metal slabs have been extensively studied and widely used in many countries for a number of years (Johnson *et al.* 2004, Al-deen *et al.* 2011, Amadio *et al.* 2004, Leon and Lange 2004, Leon *et al.* 2008). However, the profiled steel sheetings require shops with a special moulding machine and specific prefabricating procedures, and consequently the thickness of the profiled steel sheeting is always limited to about

---

∗Corresponding author, Ph.D. Student, E-mail: yyllyp126@sina.com

2 milometers. As a result, if temporary scaffoldings are not used for sustaining the construction loads, the slab spans are always limited to small spans, and a large quantity of secondary beams are subsequently needed for a sizeable space. If temporary scaffoldings are adopted instead of using an excessive number of beams, the cost of labor and time for scaffolding will be high. Therefore, neither of these two methods will be cost-effective for large-span floors with thin profiled steel sheeting. In order to overcome these limitations, normal flat steel plates with greater thickness should be introduced. For normal flat steel plates, no special fabricating procedures and moulding machines are needed, and therefore the fabrication costs are much less then for profiled steel sheetings. Most importantly, flat steel plates could be easily adopted without any limitation of thickness. Consequently, spans of composite slabs could be as large as wanted, and neither too many beams nor temporary scaffoldings should be used, because of the large flexural rigidity and bending capacity of thicker steel plates with some stiffeners or ribs. Furthermore these slab systems can be produced in every steel fabrication shop, which can also result in reduced transporting time and costs. Therefore, the totally construction costs of composite slabs with flat steel plates could be substantially reduced, despite the fact that more steel materials are used compared to the composite slabs using metal slabs.

One critical problem involving this kind of flat steel plate-concrete composite slab is the shear stress transferring between the steel plate and the concrete. In most composite slabs with normal flat steel plate, shear studs are used to develop this stress transfer. Shear studs can definitely supply enough shear force resistance, in spite of strict welding requirements, and this sometimes requires more time and money. The problem involves the flexure rigidity of the flat steel plate when the concrete is still fresh and wet during the construction stage, because the flexure rigidity is only contributed by the flat steel plate and is not sufficient to sustain the weight of wet concrete of big span slabs, which will also result in small spans like metal slabs.

The authors have recently conducted a series of experiments on a new type of composite slab named flat steel plate-concrete composite slab. As illustrated in Fig. 1, common flat steel plate instead of profiled steel sheeting was adopted as bottom metal slab, and the flat steel plate was connected to concrete by a type of perforbond shear connectors (abbreviated here as PBL shear connectors) instead of stud shear connectors (Hou *et al*. 2012, Yeol and Jeong 2006). During the construction stage, the PBL shear connectors could also serve as stiffeners or ribs to enhance the flat steel plates' bending capacity and flexure rigidity, with which the slab's span can be substantially enlarged. The PBL shear connectors could develop significant stress transfer between the steel and concrete so that the flat steel plate could fully serve as the reinforcing steel bars, and therefore no other reinforcement is needed. This kind of composite slab offers several significant advantages including large bending capacity and flexure rigidity, reducing cost and flexibility as well as simplifying construction and design for big spans (Allahyari *et al*. 2014, Papastergiou and Lebet 2014). A series of experiments have been conducted to study the mechanical performance of this type of composite slab (Yang *et al*. 2009, 2012). In practice, the composite slab rests on steel and therefore forms a new kind of composite beam as shown in Fig. 2, whose composite actions were achieved by the shear the studs shear connectors. Fig. 2 presents a schematic of the construction of the composite beam. This kind of flat steel plate-concrete composite slabs and the composite beams were be used in some building floors in China, and were also used in the Dongping bridge in Guangdong province in Southern China, which were showed in the Fig. 3.

Comparing to the composite deck using the profiled steel sheeting, this composite slabs mainly has three innovative ideas, which are listed as follows. Firstly, the flat steel plate was used instead of the profiled steel sheeting, and therefore can enlarge the span of the slabs with less cost.
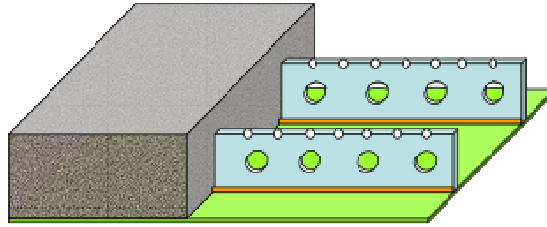
Fig. 1 The schematic of flat steel plate-concrete composite slabs

(a) Cross section
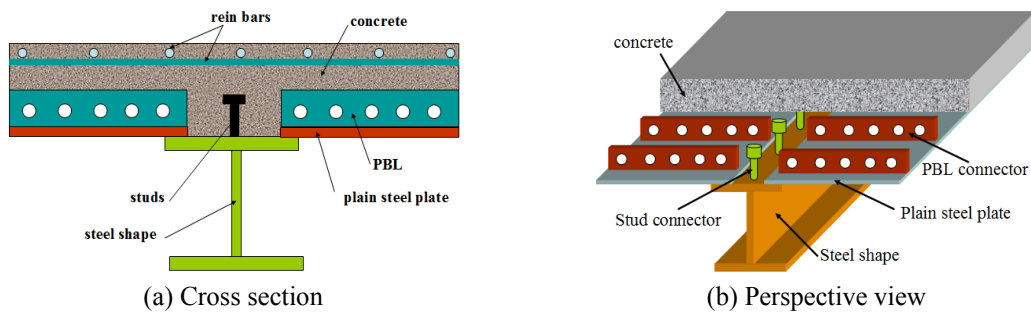
(b) Perspective view

Fig. 2 The schematic of the composite beam

(a) The panoramic view of the bridge

(b) The composite slabs of the bridge

Fig. 3 The Dongping bridge in Fushan city of Guangdong province, China

Secondly, a kind of new PBL shear connector was used in this kind of composite slabs, in which the passing-through reinforced bars were placed at the bottom edge of the holes of the PBL connectors, which were always put in the middle of the holes in other kind of PBL connectors. Thirdly, with the contribution of the fillet welding and PBL connectors, the composite action might be fulfilled even without any studs shear connectors, and therefore can largely simplify the in-site construction procedure.

In order to establish the design methods of this composite beam, the bending capacity and the flexure rigidity under positive (sagging) and negative (hogging) moment were studied by

experiments. In the experiment, two composite beam specimens based on the different engineering practices were tested: one specimen was tested under sagging bending moment, and the other one was tested under hogging bending moment, which means the specimen was turned over for testing. In order to get flexural failure under positive and negative bending moment, the parameters of the specimen CBZ and specimen CBF were different. The results of these tests provide the basis of a design method presented later in this paper.

2. Test program

2.1 Test specimens

Two composite beam specimens labeled as CBZ and CBF have similar cross-section shape and geometry dimensions. The steel shapes were Chinese steel standard shapes HM250×175, in which the thickness of web and flanges were 7 mm and 11 mm respectively, and the measured yield stress and ultimate stress of the steel shape were 303 MPa and 490 MPa. In order to avoid local buckling of the steel shape at the load points, some vertical stiffeners were adopted.

The thickness of the composite slabs in both specimens was 100 mm, the concrete of the specimens cover over the rebars is 24 mm which were designed and manufactured as scale model.

the thickness of the flat steel plate in the composite slabs was 6 mm, and the measured yield stress and ultimate stress of the flat steel plates were 310 MPa and 434 MPa. In the composite slabs of both specimens CBZ and CBF, the reinforcing steel bars at the transverse direction were arranged at spacing of 200mm with 12mm diameter, and at the longitudinal direction, the reinforcing steel bars were arranged with the total area of 1696 square mm (15 species of 12 mm diameter rebars) for specimen CBZ and 2148 square mm (19 species of 12 mm diameter rebars) for specimen CBF respectively. The measured yield stress and ultimate stress were 320 MPa and 425 MPa respectively. The concrete grades in composite slabs of two specimens were not the same: the concrete strength grade in specimen CBZ was C25 with the aim of making the whole composite slab in the compression zone to avoid concrete cracking, while the concrete strength grade of CBF was C45 with the aim of postponing the concrete cracking and therefore improving the shear capacity of the stud shear connectors in the tension zone. The test cube compression strength of concrete C25 and C45 were 23.0 MPa and 44.9 MPa respectively.

In both specimens, the PBL shear connectors were arranged at the space of 240 mm, the size of the each PBL shear connector plate was 14×70×565 mm, and the measured yield stress and the ultimate stress of the PBL plate were 304 MPa and 497 MPa respectively. A series of holes with a diameter of 40 mm were spaced at 100 mm in the PBL shear connector, and one steel bar with a diameter of 10 mm was laid through each hole in the PBL connector. Herein, the rebar combined with the concrete between the rebar and hole acted as a dowel, which could transfer the shear force between the steel plate and concrete. The diameter of the bar and the diameter of the hole both play important roles on the shear capacity of the PBL shear connectors. For the purposes of the study described in this paper, the diameter of the holes and the bars were designed according to the experimental results reported in reference (Nie *et al*. 2008, Pecce *et al*. 2012).

Specimen CBZ and specimen CBF had the same kind of stud shear connectors with the size of 16 mm-diameter and 65 mm-height, and the measured yield stress and ultimate stresses of the shear connectors were 440 MPa and 560 MPa. It should be noted that the main aim of this experiment was not to study the influence of shear connectors but rather to examine the bending capacity of the composite beams with full composite action. Therefore the stud shear connectors

Table 1 Geometry size and key parameters of specimens

Specimen No.	Span /mm	Height /mm	Width /mm	Steel shape	Studs arrangement	PBL shear connectors	Concrete compression strength /MPa
CBZ	3300	350	1200	HM250×175	Φ16×65@120	14×70×565@240	23.0
CBF	3300	350	1200	HM250×175	Φ16×65@80	14×70×565@240	44.9
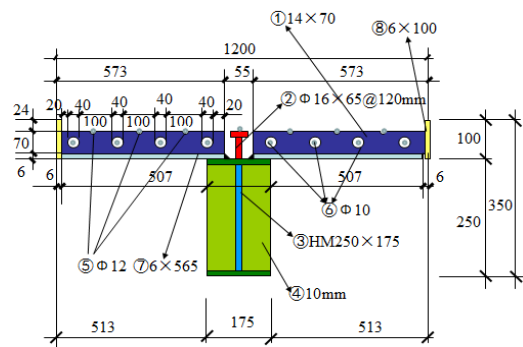
(a) Schematic of steel skeleton of specimen CBZ   (b) Photo of steel skeleton of specimen CBZ

Fig. 4 Section details of the composite beam specimen CBZ

were designed to ensure full composite action between the steel shape and the composite slab, and the spacing of the stud shear connectors were somewhat narrower than the calculated spacing of 135 mm, which was calculated by according to procedures of designing codes for other kind of steel-concrete composite beams. Considering that the shear capacity of stud shear connectors in the tension zone may be somewhat smaller than that in the compression zone, the stud shear connectors were finally laid with spacing of 120 mm in Specimen CBZ and 80 mm in specimen CBF respectively. In order to ensure sufficient connection integrity of the flat steel plate and the steel shape during the construction stage, the flat steel plates were welded to the top flange of the steel shape with 6 mm-height fillet welds. These welds acted as additional shear connectors but were ignored in the designing of specimens.

All the key size parameters and key material properties such as compression strength of concrete and arrangement of studs are listed in Table 1. The details of the specimens cross-sections are denoted in Fig. 4.

2.2 Test load-setup

Composite beam specimens CBZ and CBF were loaded under 4-point symmetric loading setup as illustrated in Figs. 5 and 6. However, specimen CBZ was placed with steel-concrete composite slabs upward (in the compression zone) and wide flange steel shape downward (in the tension zone) for investigating sagging bending (or positive bending) performance, while specimen CBF was placed in the opposite direction, with the composite slabs downward and the steel shape upward for investigating hogging bending (or negative moments) performance. Static loads were applied in the loading point position (seen in Fig. 5) by two hydraulic jacks. During the

experiments, all the deflections of the specimens at the central point, the two loading points and the two supports were measured by LVDTs. In addition, LVDTs labeled D47 and D48 were placed at two ends of the specimens to measure the slip between the steel shape and concrete slab. All the strains in the steel beam flanges and web, the flat steel plates and the concrete were measured by strain gauges. Two series of strain gauges (S17, S18, S19, S26 and S27, S28, S29, S30) were set along the height of the steel shape in both sides of the specimens at the center point as shown in Fig. 7 to verify the plane sections hypothesis. The layout of LVDTs (from D41 to D48) is presented in Figs. 5 and 6, and the locations of the strain gauges (from S1 to S30) in the specimens are presented in Fig. 7.

(a) Specimen CBZ   (b) Specimen CBF
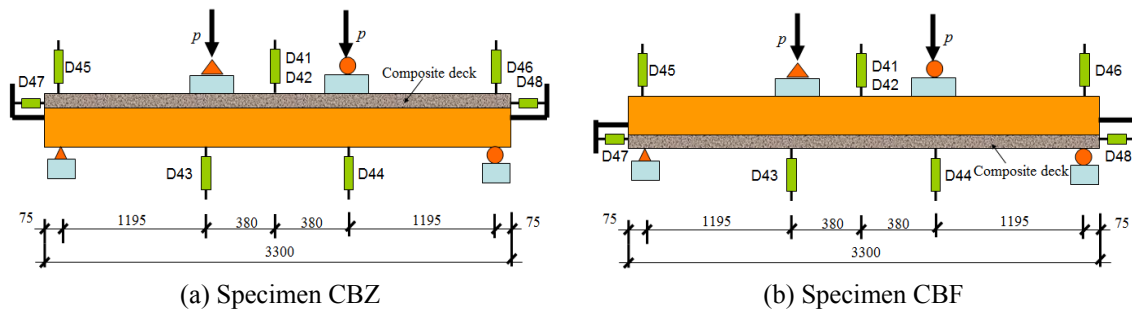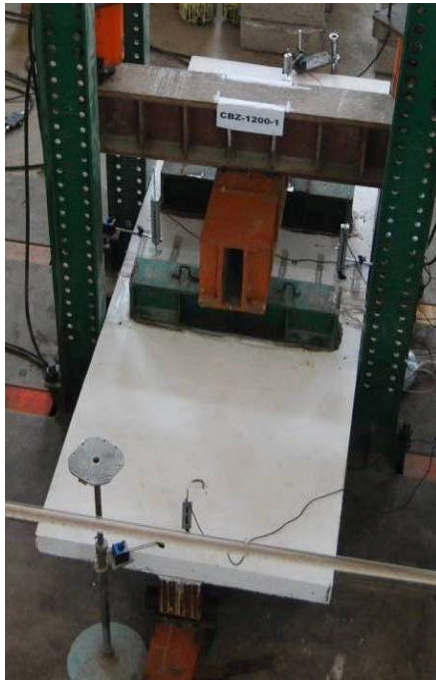
Fig. 5 Schematic of test setup of two specimens

(a) Specimen CBZ   (b) Specimen CBF
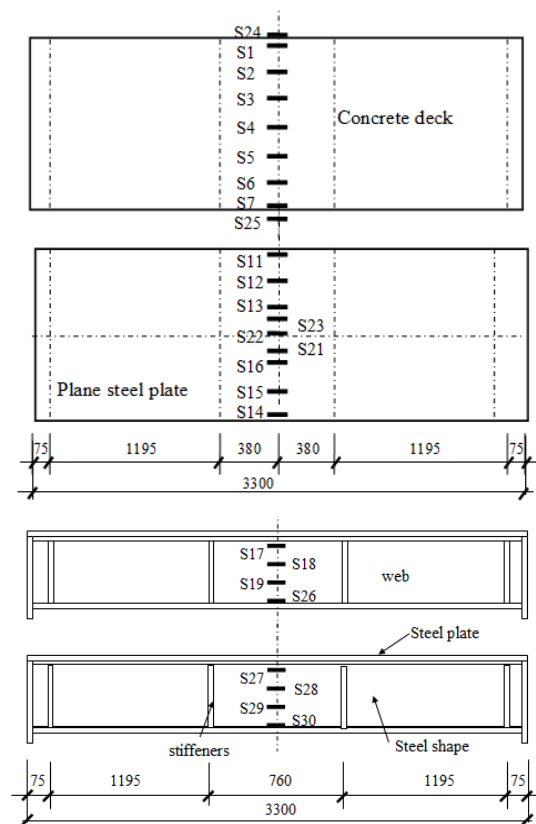
Fig. 6 Photos of test setup of two specimens

Fig. 7 Layout of the strain gauges in two specimens

2.3 Test phenomenon

Two specimens were loaded monotonically and statically by two 1000 kN hydraulic jacks. At the beginning of the test, a 5 kN force was applied firstly to check the test setup. Following that, the load was increased with load steps of 2 kN for observing and recording the cracks of the specimens.

Specimen CBZ was loaded under sagging bending moment, and concrete was mainly at the composite zone. The first batch of cracks didn't appear until the specimen was loaded to about 70% to 80% of maximum load P_u. The first batch cracks were longitudinal cracks and appeared initially near the ends of the specimens. With the load increasing, the longitudinal cracks progressed quickly toward the load points. When the specimen was loaded to 95%P_u, two new longitudinal cracks that were almost parallel to the first longitudinal cracks appeared. When the specimen was loaded to its ultimate load, P_u, the top concrete of the composite slab began to crush and drop. The deformation of the specimen increased quickly after concrete crushing, but the load decreased slowly. With increasing deformation, the concrete of the top surface at mid-span were severely crushed, the load began to decrease fast, and the experiment was stopped. Photos of the crack patterns and the final failure modes of specimen CBZ are shown in Figs. 8 and 9.

For specimen CBF, the composite slab of specimen CBF was in the tension zone, and the concrete in the composite slab was tensed and cracked very early. The cracks were sequentially
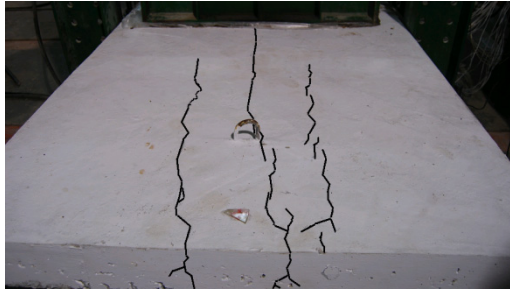
Fig. 8 Crack patterns of specimen CBZ

Fig. 9 Final failure mode of specimen CBZ

labeled from 1 to 8, and their locations are shown in Fig. 10. When the specimen was loaded to about 20%P_u, the first batch of cracks 1, 2, and 3 were observed in the mid-span cross section of the specimens, and these cracks propagated transversely. When the load increased to about 35%P_u, the second batch of cracks 7 and 8 appeared, which were almost parallel to the first batch of cracks. As the load increased to 50%P_u, some other new transverse cracks (4, 5 and 6) appeared, and with the load increasing progressively, most of the main cracks gradually caused some new tiny cracks. When the load reached P_u, the steel shape at the mid-span section was severely buckled, with the deformation increasing quickly and the load decreasing suddenly. All the cracks at the surface of composite slab are shown in Fig. 10, and the final failure modes are also shown in Fig. 11.
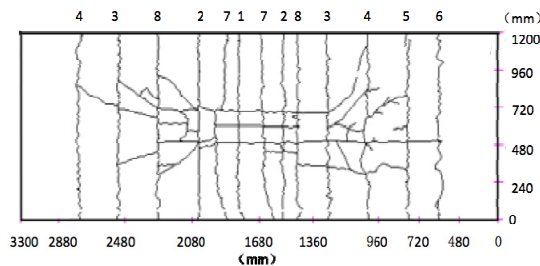
(a) Scheme of cracks

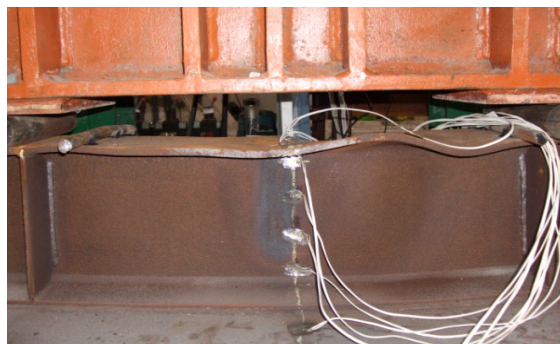(b) Photo of cracks

Fig. 10 Cracks of specimen CBF

Fig. 11 Final failure modes of specimen CBF

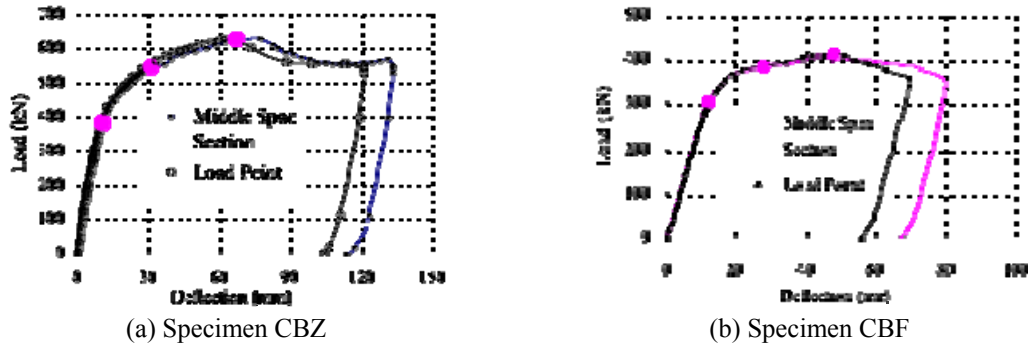(a) Specimen CBZ   (b) Specimen CBF

Fig. 12 Load vs. deflection curves of two specimens

2.4 Experimental results

The load-deflection curves of specimen CBZ and specimen CBF are presented in Fig. 12. These figures show that the failure progress of both specimens can be divided into four stages, which can be referred to as the elastic stage, the elastoplastic stage, the plastic stage and the failure stage. And from the curves, it could be also concluded that both of the two specimens had good ductility. Neither specimen failed suddenly, which demonstrated reasonable ductility and bending capacity with relatively large deflections. Ductility ratios of specimen CBZ and CBF were 5.2 and 5.4 respectively; here the deformation ductility ratios were calculated as the ultimate deflection divided by the yielding deflection, in which the ultimate deflection was the deflection when the load was $85\%P_u$ at the load-descending stage, and the yielding deflection was the deflection referring to the steel shape yielded, which was determined from the strain gauges of steel shape flanges and web.

3. Bending capacities

3.1 Basic assumptions

During the process of examining these two specimens, no obvious slipping either on the interface between flat steel plate and concrete or on the interface between steel shape and composite slab was observed, which denoted that the specimens were fully connected and composited. For this kind of composite beam, the flat steel plate and concrete in the composite slab was only connected by the PBL shear connectors. But the interaction of steel shape and composite slabs were not only attributed by the stud shear connectors but also attributed by the fillet welds between the steel shape's top flange and flat steel plate, and for safety and simplification, the fillet welds that could be regarded as additional shear connectors and not be counted in designing. The section stress and strain distribution of composite beams are shown in Fig. 13(a).

From the experimental results reported above and others research results (Nie *et al*. 2004), it could be concluded that two composite specimens were fully shear connected or fully composited. The following assumptions can be summarized from these tests:
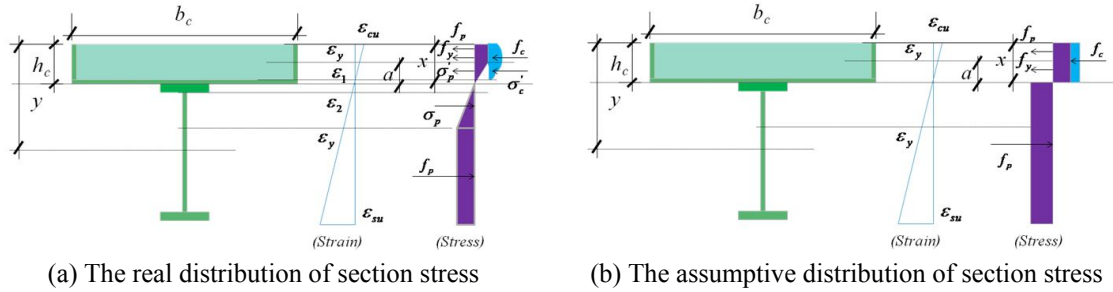
(1)   The plane-section assumption was satisfied.

(a) The real distribution of section stress   (b) The assumptive distribution of section stress

Fig. 13 The section stress and strain distribution of composite beams

(2) The composite beam was ductile, and the cross section could be considered as in wholly plastic state, and therefore the stresses of steel shape at both the tension zone and the compression zone could be taken as yield stress, as illustrated in Fig. 13(b).

(3) The tension strength of the concrete was relatively small and was therefore neglected.

(4) The stress of the concrete at the compressive zone could reach its design compressive strength and the rectangle stress block method could be used.

3.2 Design procedure

3.2.1 Bending capacity under sagging moment

For the composite beams under sagging moment, the bending capacity varies for the variation of neutral axis, and in order to simplify the design procedure, two different cases could be defined as the following, which are also denoted in Fig. 14. For simplification, the contribution of two side plates in the composite beam specimens with area of A_{cc} was not taken into account.

(1) Case 1: Neutral axis passes through the composite slabs

When the height of the compression zone x is smaller than h_c, it is considered that the steel beam and bottom steel plate is tensed to yielding stress. The following equations can be obtained from equilibrium conditions. The bending capacity of composite beams can be calculated from Eq. (1).

$$M_u = A_b f_p \left[h - \frac{1}{2} t_s - \frac{x}{2} \right] + A_s f_p \left[h - \frac{1}{2} h_s - \frac{x}{2} \right] + A_{cx} f_p \left[h_c + \frac{1}{2} t_{cx} - \frac{x}{2} \right]$$
$$+ A_u f_p \left[h_c + \frac{1}{2} t_s + t_{cx} - \frac{x}{2} \right] - A'_{s1} f'_y (a'_{s1} - \frac{x}{2}) - A'_{s2} f'_y (a'_{s2} - \frac{x}{2}) \tag{1}$$

Where x is the calculation depth of the compression zone of concrete, and can be calculated by Eq. (2).

$$x = \frac{\left[A_b + A_s + A_u + A_{cx} \right] f_p - A'_{s1} f'_y - A'_{s2} f'_y}{b_c f_{cm}} \le h_c \tag{2}$$

(2) Case 2: Neutral axis passes through web of steel shape

When the height of the compression zone x is larger than $h_c + t_{cx}$, it is considered that the steel shape above the axis and the composite slab are in the compression state and yielded. The following equations can be obtained from equilibrium conditions. The bending capacity of

composite beams can be calculated as the Eq. (3).

$$
\begin{aligned}
M_u = &A_b f_b (h - \frac{1}{2} t_s - \frac{1}{2} h_c) + (A_s - A_{s1}) f_p \frac{h - t_s + x - h_c}{2} - A_{s1} f_p \frac{x + t_{cx} + t_s}{2} \\
&- A_u f_p (\frac{1}{2} t_s + t_{cx} + \frac{1}{2} h_c) - A_{cx} f_p \frac{t_{cx} + h_c}{2} - A'_{s2} f'_y (a'_{s2} - \frac{1}{2} h_c) - A'_{s1} f'_y (a'_{s1} - \frac{1}{2} h_c)
\end{aligned}
\tag{3}
$$

Where x can be calculated by Eq. (4).

$$
x = \left[\frac{\left(A_b + \frac{h + h_c}{h_f} A_s - A_u - A_{cx} \right) f_p}{2 A_s f_p} - \frac{A'_{s1} f'_y + A'_{s2} f'_y + b_c h_c f_{cm}}{2 A_s f_p} \right] \times h_f \geq h_c
\tag{4}
$$

(3) Case 3:Neutral axis is across the bottom steel plate of composite slabs

When the height of the compression zone x is larger than h_c and smaller than $h_c + t_{cx}$, it is considered that the steel shape is tensed to yielding stress. The following equations can be obtained from equilibrium conditions. The bending capacity of composite beams can be calculated from Eq. (5).

$$
\begin{aligned}
M_u = &A_b f_b (h - \frac{1}{2} t_s - \frac{1}{2} h_c) + A_s f_p (h - \frac{1}{2} h_s - \frac{1}{2} h_c) + A_u f_p (\frac{1}{2} t_s + t_{cx} + \frac{1}{2} h_c) \\
&+ A_{cx2} f_p \frac{t_{cx} + x}{2} - A_{cx1} f_p \frac{x}{2} - A'_{s2} f'_y (a'_{s2} - \frac{x}{2}) - A'_{s1} f'_y (a'_{s1} - \frac{x}{2})
\end{aligned}
\tag{5}
$$

Where x can be calculated by Eq. (6).

$$
x = \frac{\left(A_b + A_s + A_u + \frac{2 h_c + t_{cx}}{t_{cx}} A_{cx} \right) f_p}{2 A_{cx} f_p} - \frac{A'_{s1} f'_y + A'_{s2} f'_y + b_c h_c f_c}{2 A_{cx} f_p} \geq h_c
\tag{6}
$$

3.2.2 Bending capacity under hogging moment

For the composite beams under hogging moment, the bending capacity also varies for the

(a) Case 1: Neutral axis is across composite slabs   (b) Case 2: Neutral axis is across steel shape   (c) Case 3: Neutral axis is right across the bottom steel plate
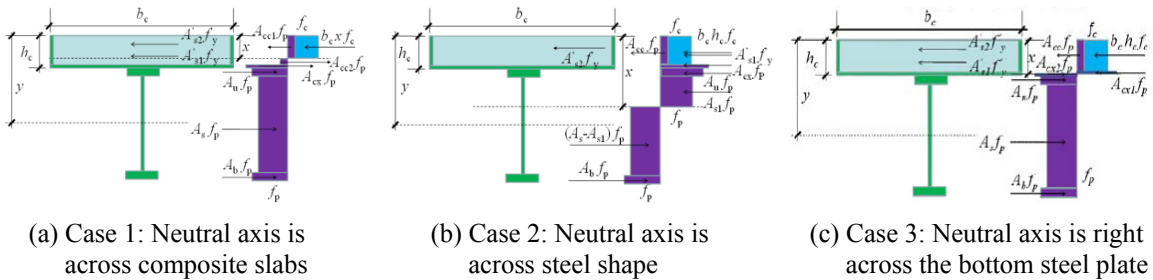
Fig. 14 Bending capacity calculation diagram of CBZ

variation of neutral axis, and two different cases could also be defined as the following, which are denoted in Fig. 15.

(1) Case 1: Neutral axis passes through composite slabs

When the height of the compression zone x is smaller than h_c, it is considered that both the steel shape and flat steel plate are compressed to yield. The following equations can be obtained from equilibrium conditions, and the bending capacity of composite beams could be calculated by the Eq. (7).

$$
\begin{aligned}
M_u = &\ A'_{s1}f'_y(a'_{s1}-\frac{x}{2}) + A'_{s2}f'_y(a'_{s2}-\frac{x}{2}) + A'_{s3}f'_y(a'_{s3}-\frac{x}{2}) - A_b f_p\left[h-\frac{1}{2}t_s-\frac{x}{2}\right] \\
&- A_{cx}f_p\left[\frac{t_{cx}}{2}+h_c-\frac{x}{2}\right] - A_u f_p\left[t_{cx}+\frac{t_s}{2}+h_c-\frac{x}{2}\right] - A_s f_p\left[t_{cx}+t_s+\frac{h_f}{2}+h_c-\frac{x}{2}\right]
\end{aligned}
\tag{7}
$$

Where x can be calculated by Eq. (8).

$$
x = \frac{\left[A_b + A_s + A_u + A_{cx}\right]f_p + b_c h_c f_{cm}}{b_c f_{cm} + \dfrac{2A_{cc}f_p}{h_c}} - \frac{A'_{s1}f'_y + A'_{s2}f'_y + A'_{s3}f'_y}{b_c f_{cm} + \dfrac{2A_{cc}f_p}{h_c}} \le h_c
\tag{8}
$$

(2) Case 2: Neutral axis passes through web of steel shape

When the height of the compression zone x is larger than $h_c + t_{cx}$, it is considered that the steel shape above the axis, the bottom steel plate, and side steel plate as well as the composite slab were all in tension state, and the steel shape underneath the axis was in the compression state. The following equations can be obtained from equilibrium conditions. The bending capacity of composite beams can be calculated by the Eq. (9).

$$
\begin{aligned}
M_u = &\ A'_{s3}f'_y(a'_{s3}-\frac{1}{2}h_c) + A'_{s2}f'_y(a'_{s2}-\frac{1}{2}h_c) + A'_{s1}f'_y(a'_{s1}-\frac{1}{2}h_c) \\
&+ (A_s - A_{s1})f_p\frac{t_s+x+t_{cx}}{2} + A_b f_b(t_{cx}+\frac{1}{2}t_s+\frac{1}{2}h_c) - A_{s1}f_p\frac{h+x-t_s-h_c}{2} \\
&+ A_{cx}f_p\frac{t_{cx}+h_c}{2} - A_u f_p(h-\frac{1}{2}t_s-\frac{1}{2}h_c)
\end{aligned}
\tag{9}
$$

Where x can be calculated by Eq. (10).

$$
x = \frac{\left(\dfrac{t_{cx}+h_c-h}{h_f}A_s + A_u - A_b - A_{cx} - A_{cc}\right)f_p \times h_f}{2A_s f_p} - \frac{A'_{s1}f'_y + A'_{s2}f'_y + A'_{s3}f'_y}{2A_s f_p} \times h_f \ge h_c
\tag{10}
$$

(3) Case 3: Neutral axis is across the bottom steel plate of composite slabs

When the height of the compression zone x is larger than h_c and smaller than $h_c + t_{cx}$, it is considered that the partial steel plate and the composite slab were all in tension state. The

following equations can be obtained from equilibrium conditions. The bending capacity of composite beams can be calculated from Eq. (11).

$$
\begin{aligned}
M_u = & A_b f_b (h - \frac{1}{2}t_s - \frac{1}{2}h_c) + A_s f_p (h - \frac{1}{2}h_s - \frac{1}{2}h_c) + A_u f_p (\frac{1}{2}t_s + t_{cx} - \frac{1}{2}h_c) \\
& + A_{cx2} f_p \frac{2x - h_c}{2} - A_{cx1} f_p \frac{x}{2} - A'_{s2} f'_y (a'_{s2} - \frac{x}{2}) - A'_{s1} f'_y (a'_{s1} - \frac{x}{2})
\end{aligned}
\tag{11}
$$

Where x can be calculated by Eq. (12).

$$
x = \frac{\left(A_b + A_s + A_u + \dfrac{2h_c + t_{cx}}{t_{cx}} A_{cx} \right) f_p}{2 A_{cx} f_p} - \frac{A'_{s1} f'_y + A'_{s2} f'_y + A'_{s3} f'_y}{2 A_{cx} f_p} \geq h_c
\tag{12}
$$

In all the equations above, the variables are defined as the following:

y is the distance between the centroid of the steel shape and the surface of the composite slab;
A'_{s1} is the area of the section of the steel bars in the bottom of the composite slab;
A'_{s2} is the area of the section of the steel bars in the middle of the composite slab;
A'_{s3} is the area of the section of the steel bars at the top of the composite slab;
b_c is the width of the composite slab of the composite beam;
t_{cx} is the thickness of the bottom steel plate of the composite slab;
t_c is the thickness of the web of the steel shape;
A_u, A_b are the areas of the upper and the bottom flange of the steel shape, respectively;
A_s is the area of the web of the steel shape;
A_{s1} is the area of the steel web that is above the neutral axis, and can be calculated by Eq. (13)

$$
A_{s1} = \frac{x - h_c - t_{cx} - t_s}{h_f} A_s ;
\tag{13}
$$

A_{s2} is the area of the steel web that is beneath the neutral axis, and can be calculated by Eq. (14)

(a) Case 1: Neutral axis is across composite slabs   (b) Case 2: Neutral axis is across the steel beam   (c) Case 3: Neutral axis is right across the bottom steel plate
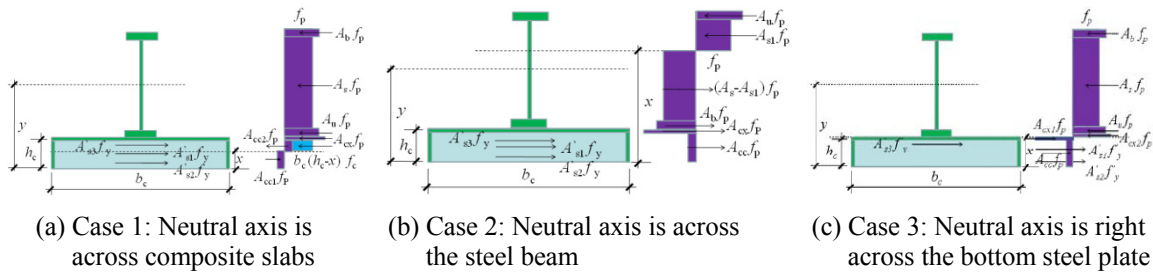
Fig. 15 Bending capacity calculation diagram of CBF

$$A_{s2} = A_s - A_{s1} = \frac{h - x - t_s}{h_f} A_s ; \qquad (14)$$

A_{cx} is the area of the bottom steel plate of the composite slab;
f_p is the design value of yield strength of the steel plate or steel beam;
f'_y is the design value of yield strength of the steel bar;
f_c is the compressive strength of the concrete;
h_s is the height of the steel shape;
a'_{s1}, a'_{s2} and a'_{s3} are the distances from the surface of the concrete flange to the centroid of the bottom steel bar, the intermediate steel bar and the upper steel bar respectively.

3.3 Verification of the design procedure

Based on design procedure described above, the bending capacity of composite beams both under the sagging moment and hogging moment were easily calculated. The calculated result of the bending capacity of specimen CBZ was 349.4 kN·m, and the tested result of that was 376.4 kN·m, which were in good agreement. The calculated result of bending capacity of specimen CBF was 286.9 kN·m, and the tested result of that was 284.4 kN·m, which were also in good agreement. Therefore, the bending capacity of this kind of composite beam can be calculated by the proposed calculation equations.

4. Conclusions

Two specimens labeled CBZ and CBF of composite beams with flat steel plate-concrete composite slabs were tested, and the performances of the composite beam under hogging and sagging bending moments were both examined. The following conclusions can be drawn from these experiment results.

(1) Specimen CBZ was tested under sagging bending moment and specimen CBF was tested under hogging bending moment. Both specimens failed in flexural failure modes, and behaved very well with large bending capacity, flexure rigidity, and good ductility.
(2) The two specimens were first designed and connected with full composite action, which was verified by the experimental results that showed no measurable slip between the interface of steel shape, flat steel plate and concrete. For this kind of composite beam, the composite action of steel shape and composite slabs was mainly attributed by the stud shear connectors, and was also enhanced by the fillet welds joining the flat plate to the beam flange, although it could be ignored for safety and simplification reasons.
(3) The plane-section assumption was verified by experimental observation and measuring slippage and strains of the cross section, and therefore bending capacity of this kind of composite beam both under hogging and sagging bending moment could be analyzed based on the plane-section assumption.
(4) Based on the plane-section assumption, a set of methods for calculating bending capacities of this kind of composite beam both under sagging and hogging bending moment was proposed, and the bending capacities of two specimens were calculated, which were in good agreement with the tested results.
(5) The shear connectors played very important roles in the mechanical performance of this

kind of composite beam, and further research should be focused on the design of the shear connectors, as well as the contribution of the fillet welds between flat steel plate and steel shape.

Acknowledgments

References

Al-deen, S., Ranzi, G. and Vrcelj, Z. (2011), "Full-scale long-term experiments of simply supported composite beams with solid slabs", *J. Constr. Steel Res.*, **67**(3), 308-321.
Allahyari, H., Dehestani, M., Beygi, M.H.A., Neya, B.N. and Ebrahim, R. (2014), "Mechanical behavior of steel-concrete composite decks with perfobond shear connectors", *Steel Compos. Struct., Int. J.*, **17**(3), 339-358.
Amadio, C., Fedrigo, C., Fragiacomo, M. and Macorini, L. (2004), "Experimental evaluation of effective width in steel-concrete composite beams", *J. Constr. Steel Res.*, **60**(2), 199-220.
Hou, Z., Xia, H. and Zhang, Y.L. (2012), "Dynamic analysis and shear connector damage identification of steel-concrete composite beams", *Steel Compos. Struct., Int. J.*, **13**(4), 327-341.
Johnson, R.P. (2004), *Composite Structures of Steel and Concrete: Beams, Slabs, Columns, and Frames for Buildings*, Blackwell Publication, USA.
Leon, R.T. and Lange, J. (2004), "Composite construction in steel and concrete V", *Proceedings of the 5th International Conference*, Berg-en-Dal, South Africa, July.
Leon, R.T., Rassati, G.A., Perea, T. and Lange, J. (2008), "Composite construction in steel and concrete VI", *Proceedings of the 2008 Composite Construction in Steel and Concrete Conference*, Tabernash, CO, USA, July.
Nie, J., Fan, J. and Cai, S.C. (2004), "Stiffness and deflection of steel–concrete composite beams under negative bending", *J. Struct. Eng.*, **130**(11), 1842-1851.
Nie, J., Fan, J. and Cai, C.S. (2008), "Experimental study of partially shear-connected composite beams with profiled sheeting", *Eng. Struct.*, **30**(1), 1-12.
Papastergiou, D. and Lebet, J.P. (2014), "Investigation of a new steel-concrete connection for composite bridges", *Steel Compos. Struct., Int. J.*, **17**(5),573-599.
Pecce, M., Rossi, F., Bibbò, F.A. and Ceroni, F. (2012), "Experimental behaviour of composite beams subjected to a hogging moment", *Steel Comp. Struct., Int. J.*, **12**(5), 395-412.
Yang, Y., Zhu, G., Zhou, P. and Nie, J. and Xie, B. (2009), "Experimental study on the mechanical behavior and design method of plane steel-plate and concrete composite bridge decks", *China Civil Eng. J.*, **42**(12), 135-141. [In Chinese]
Yang, Y., Zhou, X., Xue, J. and Huo, Z. (2012), "Experimental study on fatigue behavior of composite girders with steel plate-concrete composite decks", *China Civil Eng. J.*, **45**(6), 123-131. [In Chinese]
Yeol, H. and Jeong, Y.J. (2006), "Experimental investigation on behavior of steel–concrete composite bridge decks with perfobond ribs", *J. Constr. Steel Res.*, **62**(5), 463-471.

CC